Resonant 4f photoelectron diffraction: Insight into Yb compounds

D. Yu. Usachov [1,2,3,*] G. Poelchen [4] I. I. Tupitsyn,[1] K. A. Bokai [1,2] D. Glazkova,[1] A. V. Tarasov,[1,2] M. Mende,[4]
A. V. Fedorov,[5] V. S. Stolyarov,[2,3] C. Krellner [6] and D. V. Vyalikh [7,8,†]

[1]*St. Petersburg State University, 7/9 Universitetskaya Naberezhnaya, St. Petersburg 199034, Russia*
[2]*Moscow Institute of Physics and Technology, Institute Lane 9, Dolgoprudny 141701, Russia*
[3]*National University of Science and Technology MISIS, Moscow 119049, Russia*
[4]*Institut für Festkörper- und Materialphysik, Technische Universität Dresden, D-01062 Dresden, Germany*
[5]*Helmholtz-Zentrum Berlin für Materialien und Energie, D-12489 Berlin, Germany*
[6]*Kristall- und Materiallabor, Physikalisches Institut, Goethe-Universität Frankfurt, Max-von-Laue Strasse 1,
D-60438 Frankfurt am Main, Germany*
[7]*Donostia International Physics Center (DIPC), E-20018 Donostia/San Sebastián, Basque Country, Spain*
[8]*IKERBASQUE, Basque Foundation for Science, E-48013 Bilbao, Spain*

Resonant photoelectron diffraction (RPED) and its use for studies of lanthanides are presented. To demonstrate the potential of this technique, we show how the ground-state properties of the heavy-fermion compound $YbRh_2Si_2$ and its trivalent counterpart $YbCo_2Si_2$ can be determined from RPED measurements and modeling. By providing a modeling recipe and exploring RPED capabilities and limitations, we anticipate wide applications of this method for insights into the properties of lanthanide-based systems.

Photoelectron diffraction (PED) is an efficient method for the comprehensive structural analysis of crystalline surfaces, impurities and defects, thin films, low-dimensional materials, as well as systems consisting of repeated, but not necessarily periodic, structural blocks [1–8]. PED is based on the photoemission (PE) of electrons from selected atomic sites, called emitters. On their way to the surface, photoelectrons undergo multiple scattering on the atoms which surround the emitter. As a result, the angular distribution of the measured photocurrent exhibits a diffraction pattern, which contains information about the properties of emitters and the local structure around them. PED also allows to explore magnetic ordering [9–11], estimate the intermixing of elements between different atomic sites [12], and determine the noninteger valency of $4f$ elements in individual atomic layers [11].

To resolve the fine structure of PED patterns, it is essential to have an intense PE signal. For certain cases, such as the investigation of deep atomic layers and dilute species, the possibility of enhancing the measured PE signal becomes of primary importance. The desired enhancement can be reached by using resonant PED (RPED) [13], where photon energy is tuned to the absorption edge of a chosen core shell [6,13,14]. Interference of the direct PE channel and the autoionization (Auger) channel may significantly amplify the PE signal. However, in the modeling of RPED patterns the latter indirect PE channel is commonly ignored [6]. This approach may lead to errors which are largely unexplored. Examples of theoretical modeling of RPED remain very few in number [10,15].

Here, we show the advances of RPED for lanthanide research. Starting with a theoretical overview of RPED, we further show how this technique allows to probe the ground-state properties of the heavy-fermion compound $YbRh_2Si_2$ influenced by a crystal electric field (CEF). We discuss the possible limitations of RPED and ways to overcome them. Namely, on the next example of $YbCo_2Si_2$ [16] we consider the case when the CEF splitting of $4f$ states is so small that several states contribute to the PE signal. Finally, we present a route for RPED modeling and discuss the consequences of ignoring the indirect PE channel.

The samples were grown according to Refs. [17,18]. Angle-resolved photoemission spectroscopy (ARPES) and RPED measurements were performed at BESSY II (One-Cubed ARPES instrument) and at the Swiss Light Source (PEARL instrument). The samples were cleaved in ultrahigh vacuum before measurements. The experimental geometry is described in the Supplemental Material [19].

To describe RPED, we use the muffin-tin model and express the PE amplitude as the sum of scattered partial waves (see Supplemental Material [19] for details)

$$\psi(\vec{k}) = 2\pi k \sqrt{\omega/c} \sum_{lm} e^{i\delta_l} \langle \chi_{klm} | \vec{\varepsilon} \cdot \vec{r} | g_0 \rangle \tilde{\psi}_{lm}(\vec{k}), \quad (1)$$

where ω is the photon energy (atomic units are used), g_0 is the atomic orbital from which the photoelectron is excited, $\vec{\varepsilon}$ is the photon polarization, δ_l is the continuum state phase shift, and χ_{klm} is the final state described by the function $\chi_{klm} = i^l r^{-1} R_{kl}(r) Y_l^m(\vec{r})$ with the radial wave function R_{kl} normalized to the delta function of energy. The photoionization cross section is $\sigma(\vec{k}) = |\psi(\vec{k})|^2$.

*Contact author: dmitry.usachov@spbu.ru
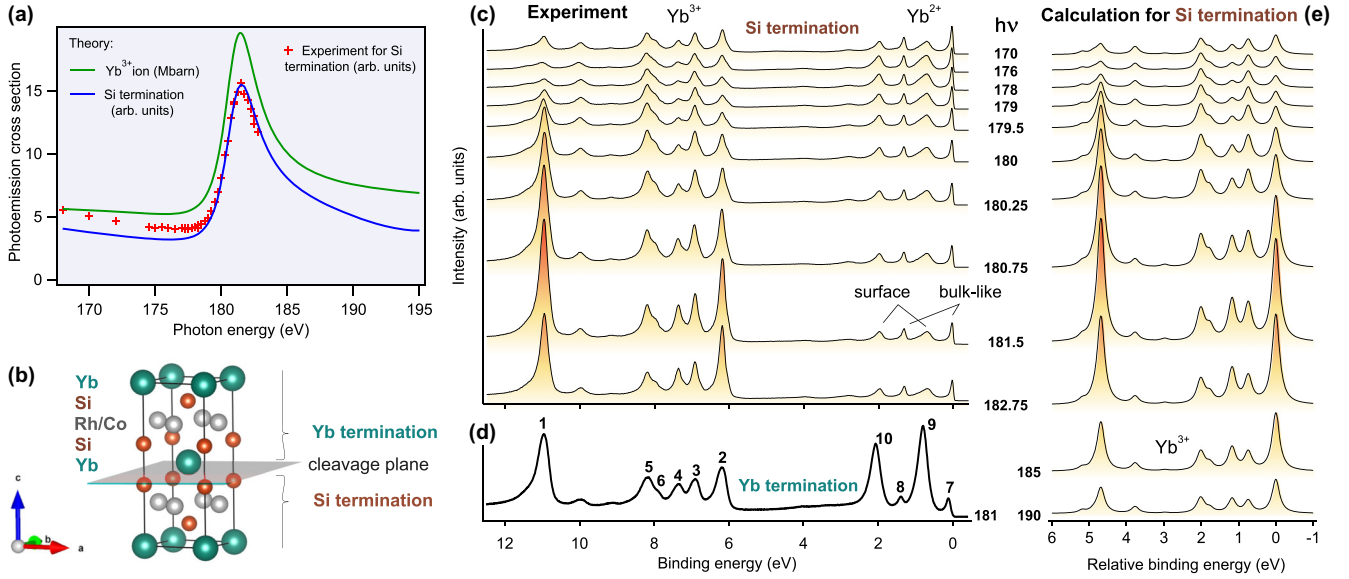†Contact author: denis.vyalikh@dipc.org

FIG. 1. Resonant PE from YbRh$_2$Si$_2$ at the Yb $4d$ threshold. (a) Yb $4f$ PE cross sections derived experimentally and theoretically. (b) Schematic presentation of the tetragonal crystal structure, cleavage plane, and possible Si and Yb surface terminations. (c) A set of PE spectra taken across the threshold from the Si-terminated surface at 2 K. (d) Resonant PE spectrum taken from the Yb-terminated surface at 2 K. (e) Computed evolution of the PE intensity of the Yb $4f^{12}$ final state multiplet across the Yb $4d$ threshold for the Si-terminated crystal.

The next step is to replace the one-electron PE matrix element in Eq. (1) by the many-electron one, taking into account the resonance. Such a matrix element for the resonant transition from the ground state $|g\rangle$ to the final state $|k\beta\rangle = |\beta, klmm_s\rangle$, with β being the final state of the ion, is given by [20]

$$\langle k\beta|T|g\rangle \approx \langle k\beta|V_r|g\rangle + \sum_{\alpha\alpha'}\langle k\beta|V_a|\alpha\rangle\langle\alpha|G_a|\alpha'\rangle\langle\alpha'|V_r|g\rangle,$$

(2)

where G_a is the Green's function of the Hamiltonian with a configuration interaction V_a, α denotes intermediate states, and V_r describes the interaction with photons.

Exemplarily, we will examine RPED at the $4d \to 4f$ absorption edge of lanthanides, focusing on two Yb-based compounds. Notably, Yb exhibits two distinct $4f$ configurations, namely $4f^{14}$ (Yb^{2+}) and $4f^{13}$ (Yb^{3+}), but only the Yb^{3+} configuration yields a resonance due to the complete occupation of the $4f$ shell in Yb^{2+}. Additionally, in heavy lanthanides the PE process is effectively characterized by the $4d \to 4f$ excitation and the super-Coster-Kronig decay channel $\langle 4d^9 4f^{n+1}|V_a|4d^{10}4f^{n-1}, kl\rangle$, which is the only decay channel we consider here. For light lanthanides, however, more decay channels must be taken into account [20].

In our calculations for Yb^{3+} ions, we limit the basis for the ground state to the $|M_J\rangle$ states of the lowest-energy term $^2F_{7/2}$,

$$|g^\nu\rangle = \sum_{M_J} A^\nu_{M_J}|4f^{13}LSJM_J\rangle.$$

(3)

To describe the intermediate states α, we use the full basis of the $|4f^{14}4d^9 L_t S_t J_t M_{Jt}\rangle$ states and diagonalize the Hamiltonian with the Coulomb and spin-orbit (SO) terms. The final states $k\beta$ were constructed from the $|4f^{12}L_f S_f J_f M_{Jf}, klmm_s\rangle$ basis states with l taking all possible values (0, 2, 4, 6, 8); the Hamiltonian parameters are given in Ref. [21]. All necessary

radial matrix elements and phase shifts are calculated with our Hartree-Fock code [22]. The scattering amplitudes $\tilde{\psi}_{lm}(\vec{k})$ are calculated with the modified version of the EDAC code [23], where we replaced the charge density of Yb with the one calculated with our code [22]. Finally, the matrix elements $\langle k\beta|V_a|\alpha\rangle$ are scaled by the factor of 0.75 to fit the experimentally measured width of the resonance.

First, it is worth establishing how well the resonant PE is described by our modeling. We show this in Fig. 1 with YbRh$_2$Si$_2$ as an example. Note that YbRh$_2$Si$_2$ and YbCo$_2$Si$_2$ expose two possible surface terminations upon cleaving, namely the Yb and Si terminations as shown in Fig. 1(b) [24,25]. Figure 1(c) shows a set of PE spectra taken across the Yb $4d$ threshold from the Si-terminated surface. Due to the noninteger valency of Yb in YbRh$_2$Si$_2$, the PE spectra reveal a coexistence of the Yb^{2+} and Yb^{3+} multiplets [26]. Note that between 0 and 2 eV of binding energy (BE), two Yb^{2+} PE doublets can be seen. They reflect the signals from the outermost Yb surface and bulklike Yb marked in Fig. 1(c). The spectral structure of a Yb^{3+} bulklike multiplet between 5 and 13 eV BE was discussed in Ref. [27].

When we change the photon energy across the Yb $4d$ threshold, the PE intensity of the Yb^{3+} multiplet is resonantly enhanced as seen from Fig. 1(c). Its evolution along with the calculated PE cross sections is shown in Fig. 1(a). The computed PE spectra of the Yb^{3+} multiplet are given in Fig. 1(e). A good agreement between the calculated and measured spectra as well as the PE cross sections is achieved when the resonance energy $E_\alpha - E_g$ is set to 181.05 eV in Eq. (2).

Shifting now our focus to the RPED measurements [Fig. 2(b)], we will show how this technique may be effectively employed to analyze the ground state of YbRh$_2$Si$_2$. The CEF with the tetragonal point symmetry splits the $J = \frac{7}{2}$ state of Yb^{3+} into four doubly degenerate states [25]. They belong
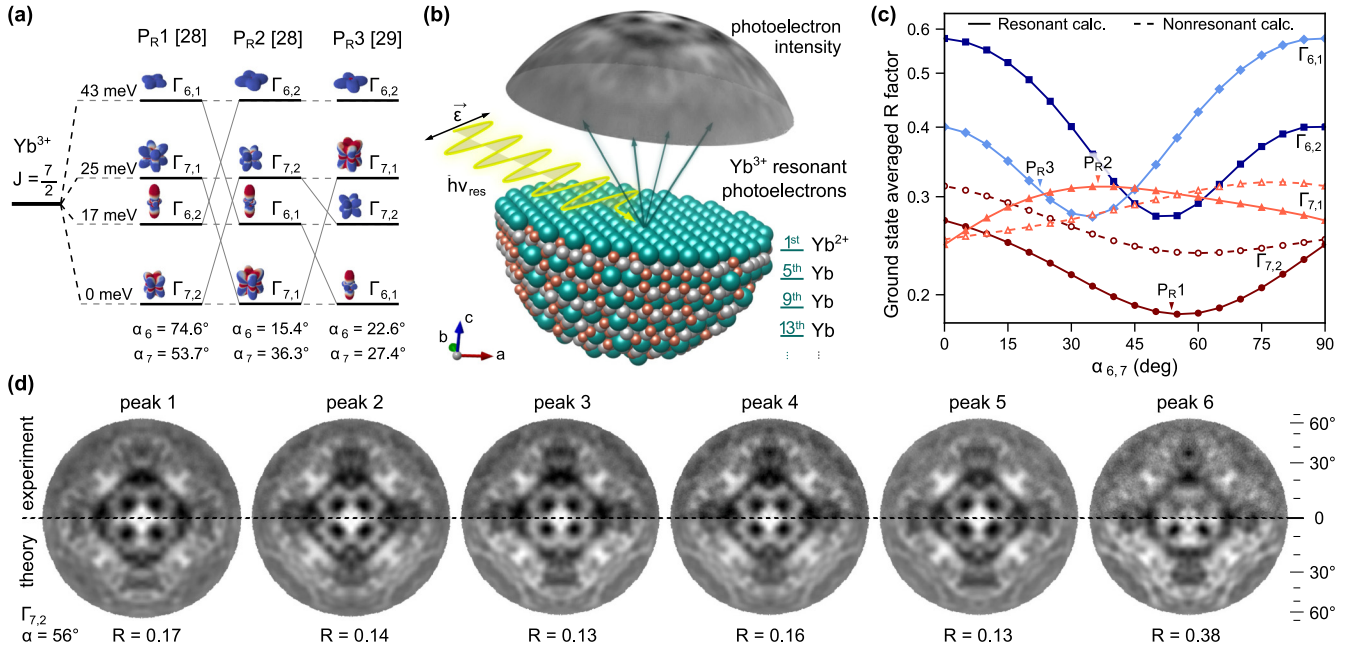
FIG. 2. (a) Different CEF schemes of YbRh$_2$Si$_2$ proposed in Refs. [28,29]. Difference in the charge densities of the closed $4f$ shell and the CEF states is illustrated (color denotes spin). (b) Schematic of the RPED experiment. (c) Average R factor of the six analyzed peaks shown in (d) for the four different ground-state configurations. Dotted lines with open symbols show the R factor when the resonant process is not taken into account. (d) Experimental and theoretical Yb^{3+} RPED patterns (with $\hbar\omega = 181$ eV at 35 K) for the peaks marked in Fig. 1(d). The PE intensity is presented in an orthographic projection with a subtracted background. The dark color corresponds to low PE intensity.

to the two irreducible representations Γ_{t6} and Γ_{t7}, leading to nonzero coefficients $A_{M_J}^\nu$ in Eq. (3) only for M_J that differ by 4. These states can be parametrized [18] as

$$\Gamma_{6,1} = \cos\alpha_6 \, |\pm 1/2\rangle + \sin\alpha_6 \, |\mp 7/2\rangle,$$
$$\Gamma_{6,2} = \sin\alpha_6 \, |\pm 1/2\rangle - \cos\alpha_6 \, |\mp 7/2\rangle,$$
$$\Gamma_{7,1} = \cos\alpha_7 \, |\pm 3/2\rangle - \sin\alpha_7 \, |\mp 5/2\rangle,$$
$$\Gamma_{7,2} = \sin\alpha_7 \, |\pm 3/2\rangle + \cos\alpha_7 \, |\mp 5/2\rangle, \qquad (4)$$

where we restrict the parameters α_6 and α_7 to the range from $0°$ to $90°$. The CEF splittings, known from neutron scattering measurements, and the proposed CEF schemes [28,29] are summarized in Fig. 2(a).

In Fig. 2(d), we show the RPED patterns from Yb-terminated crystal for the peaks 1–6 marked in Fig. 1(d). Since the PED matrix element is mostly determined by the crystal structure, all patterns reveal similar sets of features. However, there are notable differences in the intensities of these features (see Fig. S1 [19]), which contain information about the ground state of Yb.

In our model, we considered the Yb^{3+} PE signal from three Yb layers (the fifth, ninth, and 13th atomic layers) below the divalent Yb surface [Fig. 2(b) and Ref. [19]]. The studies of structurally similar LnRh$_2$Si$_2$ systems (Ln = Tb, Dy, and Ho) [30,31] revealed a strong relaxation of the trivalent Ln termination which should be considered in modeling. However, for the divalent Yb surface of YbRh$_2$Si$_2$ PED patterns modeled without relaxation agree well with experiment, indicating no significant relaxation. This is supported by our density functional theory (DFT) calculations, where the derived displacements of atoms near the surface are negligible (<0.07 Å

relative to their positions in the bulk; see Fig. S2 and related discussion in Supplemental Material [19]).

Since for YbRh$_2$Si$_2$ the $4f$ ground-state doublet is separated by 17 meV from the first excited doublet, we can neglect the occupation of excited states at the temperature of RPED experiment ($\sim$35 K). To establish the ground state of YbRh$_2$Si$_2$, we examined all four possible doublets given by Eq. (4) with all possible values of α_6 or α_7. Each modeled RPED pattern was compared with the experimental one by means of a reliability factor R defined in Ref. [32]. In Fig. 2(c), we present the dependencies of the R factor which was averaged over six RPED patterns for all four possible ground states. As seen, the optimal ground state, corresponding to the global minimum of R, is $\Gamma_{7,2}$ with $\alpha_7 = 56°$. It agrees perfectly with the ground state corresponding to the CEF parameters P_R1, proposed in Ref. [28] along with the P_R2 set. They both were derived from the analysis of inelastic neutron scattering and electron paramagnetic resonance measurements. However, no decision was made as which of the two sets is the decisive one. As we can see now, the RPED data allow us to make the final statement.

It is worth noting that the RPED patterns in Fig. 2(d) reveal R factors smaller than 0.2, implying a good agreement between experiment and theory. The only exception is peak 6, which shows a large R value due to its low intensity and, consequently, noisy pattern. Nevertheless, its R factor reaches a minimum close to the P_R1 parameters.

It is instructive to analyze the consequences of disregarding the indirect term in the PE matrix element. For this case, the calculated dependencies of the R factor for the Γ_7 ground states are shown by dashed lines in Fig. 2(c). One can see that the R-factor curve for $\Gamma_{7,2}$ is shifted by more than 40% to
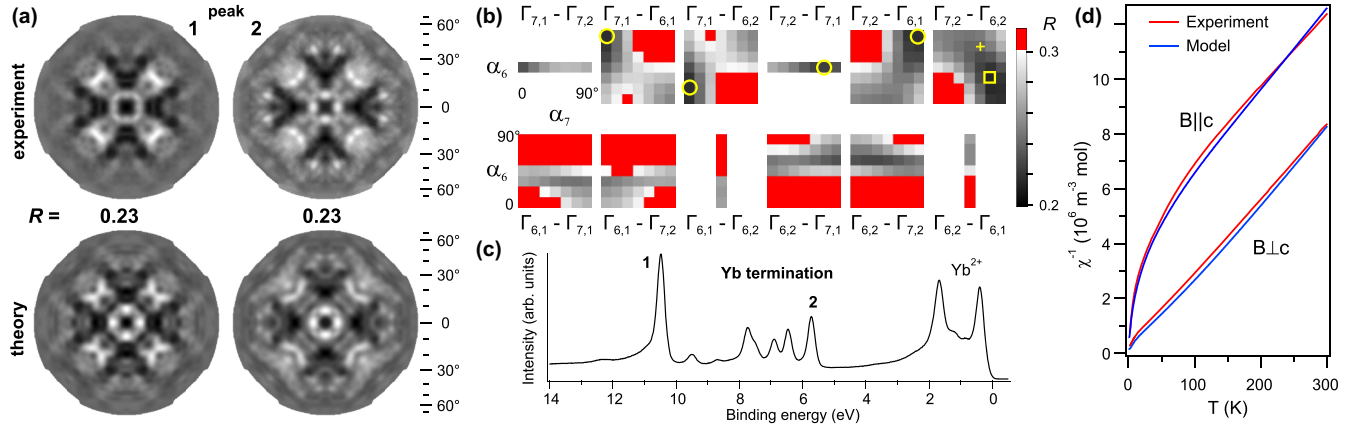
FIG. 3. (a) Experimental and theoretical RPED patterns from the Yb^{3+} $4f$ multiplet of $YbCo_2Si_2$ for the peaks marked in (c). Measurements were conducted at $\sim$35 K and calculations were performed with CEF parameters P_C3. (b) R-factor dependence on the parameters of $4f$ states for different CEF schemes. (c) PE spectrum taken from the Yb termination at $h\nu = 181$ eV. (d) Measured inverse magnetic susceptibility compared with the one calculated for the CEF parameters P_C3 at the magnetic field $B = 2$ T.

larger values of R and its minimum now is less obvious and moved away from the P_R1 point. In addition, the difference in R between the sets P_R1 and P_R2 decreases as compared to the resonant curves. Overall, we conclude that ignoring the resonant term may provide a comparable but substantially less reliable result. We should add here that for certain cases (e.g., for Eu [11]), the resonance may not significantly affect the PED patterns.

We can better understand the capabilities and limitations of RPED by looking also at the trivalent compound $YbCo_2Si_2$, for which the results are summarized in Fig. 3. The PE spectrum taken from the cleaved sample reveals a high intensity of the Yb^{2+} doublet [Fig. 3(c)] implying that the sample surface is mostly Yb terminated. The PED analysis indicates the possible presence of about 10% of a Si-terminated surface that does not affect the results. Compared to the spectrum for $YbRh_2Si_2$, this one lacks peaks 7 and 8. This is a spectroscopic signature of trivalent behavior of Yb in the bulk of $YbCo_2Si_2$ [16]. For measurements, we considered the highest-intensity peaks marked as 1 and 2. The obtained RPED patterns are shown in Fig. 3(a). As for $YbRh_2Si_2$, we first considered only the ground-state doublet. RPED analysis indicates that the optimal ground state is $\Gamma_{7,2}$. The dependence of $R(\alpha_7)$ looks similar to the corresponding curve in Fig. 2(c), but with smaller variations of R ranging from 0.34 to the global minimum of 0.25 reached at $\alpha_7 = 68°$ (see Fig. S3 [19]). Thus, the obtained results for $YbCo_2Si_2$ are very similar to those of $YbRh_2Si_2$.

However, as seen from Table I, the ground-state doublet of $YbCo_2Si_2$ is separated from the first excited doublet by only 4 meV [33]. Therefore, the second doublet contributes significantly to the PE signal at $\sim$35 K, that is the temperature of experiment. It is therefore necessary to consider PE from both the ground state and the first excited state, and model the wave functions for all permutations allowed by Eq. (4). Following this procedure, we derived the two-dimensional (2D) R-factor maps which are given in Fig. 3(b). The obtained global minimum of R is highlighted with a yellow square. Although it indicates that $\Gamma_{7,2}$ is the ground state, it is seen that there are several local minima (marked with yellow circles), for which the R factors differ not too much from that of the global minimum. This implies that the wave functions of the ground and first excited states cannot be uniquely identified from RPED measurements at 35 K.

This problem can be solved by performing measurements at lower temperature. If this is not accessible, with the help of data from the other techniques, it is feasible to choose appropriate wave functions not only for the two doublets, but for the entire CEF-split multiplet. In order to do this, we first computed anisotropic g factors and magnetic susceptibility and compared them with experiment [18]. Then, we searched for the CEF parameters which provide the smallest R and show good agreement for g factors and susceptibility. This approach gave us the unique solution marked by the yellow cross in Fig. 3(b) and denoted as P_C3 in Table I. The respective anisotropic susceptibility, shown in Fig. 3(d), and g factors given in Table I, agree nicely with experiment [18,34]. As we see, the obtained optimal solution is not far from the global minimum of R, but the parameter α_6 deviates notably. This can be explained by the fact that CEF near the surface

TABLE I. Characteristics of $YbCo_2Si_2$ $4f$ states. Possible CEF parameters B_q^k are given in meV for spherical tensor operators. Experimental g factors are $g_c \approx 1.4$ and $g_{ab} \approx 2.8$ [18]. The parameter set P_C3 is derived in this work.

Energy levels	Ref.	B_0^2	B_0^4	B_4^4	B_0^6	B_4^6	Scheme	α_6	α_7	g_{ab}	g_c	Label
$YbCo_2Si_2$ [33]	[33]	48.1	−19.3	−25.2	35.4	7.51	$\Gamma_{6,2} - \Gamma_{7,1} - \Gamma_{7,2} - \Gamma_{6,1}$	82.3°	42°	4.49	0.98	P_C1
	[18]	47.3	−28.5	−27.7	−12.5	2.16	$\Gamma_{7,1} - \Gamma_{6,2} - \Gamma_{7,2} - \Gamma_{6,1}$	81.7°	27°	3.20	1.54	P_C2
0,4,12.5,30.5 meV	This work	43.4	−29.5	2.38	−15.7	62.7	$\Gamma_{7,2} - \Gamma_{6,2} - \Gamma_{7,1} - \Gamma_{6,1}$	75°	62°	3.28	1.41	P_C3

may slightly differ from CEF in the bulk. Such possibility is evidenced by our studies of $LnRh_2Si_2$ compounds, where Ln = Tb, Dy, and Ho [30,31]. When the energy separation between the ground and excited $4f$ states is small, as in the case of $YbCo_2Si_2$, the influence of surface effects can be essential.

In summary, the presented RPED approach and its application to the heavy-fermion compound $YbRh_2Si_2$ illustrates a potential of exploiting the resonant PE process in PED measurements for studies of lanthanides. Especially, a conclusive determination of the ground-state properties of $YbRh_2Si_2$ as well as a discussion of RPED's limitations considered for the case of trivalent $YbCo_2Si_2$ demonstrates that RPED is a powerful spectroscopic tool for studies of heavy-fermion phenomena. It can be extended quite naturally to other strongly correlated materials and applied at other resonant excitations such as $3d \rightarrow 4f$ [35].

[1] C. S. Fadley, X-ray photoelectron spectroscopy: Progress and perspectives, J. Electron Spectrosc. Relat. Phenom. **178-179**, 2 (2010).

[2] C. Westphal, The study of the local atomic structure by means of x-ray photoelectron diffraction, Surf. Sci. Rep. **50**, 1 (2003).

[3] D. P. Woodruff, Surface structural information from photoelectron diffraction, J. Electron Spectrosc. Relat. Phenom. **178-179**, 186 (2010).

[4] F. Matsui, T. Matsushita, and H. Daimon, Holographic reconstruction of photoelectron diffraction and its circular dichroism for local structure probing, J. Phys. Soc. Jpn. **87**, 061004 (2018).

[5] M. V. Kuznetsov, I. I. Ogorodnikov, D. Y. Usachov, C. Laubschat, D. V. Vyalikh, F. Matsui, and L. V. Yashina, Photoelectron diffraction and holography studies of 2D materials and interfaces, J. Phys. Soc. Jpn. **87**, 061005 (2018).

[6] A. Verdini, P. Krueger, and L. Floreano, in *Surface Science Techniques*, edited by G. Bracco and B. Holst, Springer Series in Surface Sciences Vol. 51 (Springer, Berlin, 2013), Chap. VIII, pp. 217–248.

[7] K. Tsutsui, T. Matsushita, K. Natori, T. Muro, Y. Morikawa, T. Hoshii, K. Kakushima, H. Wakabayashi, K. Hayashi, F. Matsui, and T. Kinoshita, Individual atomic imaging of multiple dopant sites in As-doped Si using spectro-photoelectron holography, Nano Lett. **17**, 7533 (2017).

[8] D. Y. Usachov, A. V. Tarasov, F. Matsui, M. Muntwiler, K. A. Bokai, V. O. Shevelev, O. Y. Vilkov, M. V. Kuznetsov, L. V. Yashina, C. Laubschat, A. Cossaro, L. Floreano, A. Verdini, and D. V. Vyalikh, Decoding the structure of interfaces and impurities in 2D materials by photoelectron holography, 2D Mater. **6**, 045046 (2019).

[9] E. D. Tober, F. J. Palomares, R. X. Ynzunza, R. Denecke, J. Morais, Z. Wang, G. Bino, J. Liesegang, Z. Hussain, and C. S. Fadley, Observation of a ferromagnetic-to-paramagnetic phase transition on a ferromagnetic surface using spin-polarized photoelectron diffraction: Gd(0001), Phys. Rev. Lett. **81**, 2360 (1998).

[10] R. Sagehashi, G. Park, and P. Krüger, Theory of circular dichroism in angle-resolved resonant photoemission from magnetic surfaces, Phys. Rev. B **107**, 075407 (2023).

[11] D. Y. Usachov, A. V. Tarasov, S. Schulz, K. A. Bokai, I. I. Tupitsyn, G. Poelchen, S. Seiro, N. Caroca-Canales, K. Kliemt, M. Mende, K. Kummer, C. Krellner, M. Muntwiler, H. Li, C. Laubschat, C. Geibel, E. V. Chulkov, S. I. Fujimori, and D. V. Vyalikh, Photoelectron diffraction for probing valency and magnetism of $4f$-based materials: A view on valence-fluctuating $EuIr_2Si_2$, Phys. Rev. B **102**, 205102 (2020).

[12] N. V. Vladimirova, A. S. Frolov, J. Sánchez-Barriga, O. J. Clark, F. Matsui, D. Y. Usachov, M. Muntwiler, C. Callaert, J. Hadermann, V. S. Neudachina, M. E. Tamm, and L. V. Yashina, Occupancy of lattice positions probed by x-ray photoelectron diffraction: A case study of tetradymite topological insulators, Surf. Interfaces **36**, 102516 (2023).

[13] P. Krüger, S. Bourgeois, B. Domenichini, H. Magnan, D. Chandesris, P. Le Fèvre, A. M. Flank, J. Jupille, L. Floreano, A. Cossaro, A. Verdini, and A. Morgante, Defect states at the TiO_2(110) surface probed by resonant photoelectron diffraction, Phys. Rev. Lett. **100**, 055501 (2008).

[14] M. Treier, P. Ruffieux, R. Fasel, F. Nolting, S. Yang, L. Dunsch, and T. Greber, Looking inside an endohedral fullerene: Inter- and intramolecular ordering of $Dy_3N@C_{80}(I_h)$ on Cu(111), Phys. Rev. B **80**, 081403(R) (2009).

[15] F. J. García de Abajo, C. S. Fadley, and M. A. Van Hove, Multiatom resonant photoemission: Theory and systematics, Phys. Rev. Lett. **82**, 4126 (1999).

[16] M. Güttler, K. Kummer, S. Patil, M. Höppner, A. Hannaske, S. Danzenbächer, M. Shi, M. Radovic, E. Rienks, C. Laubschat, C. Geibel, and D. V. Vyalikh, Tracing the localization of $4f$ electrons: Angle-resolved photoemission on $YbCo_2Si_2$, the stable trivalent counterpart of the heavy-fermion $YbRh_2Si_2$, Phys. Rev. B **90**, 195138 (2014).

[17] C. Krellner, S. Taube, T. Westerkamp, Z. Hossain, and C. Geibel, Single-crystal growth of $YbRh_2Si_2$ and $YbIr_2Si_2$, Philos. Mag. **92**, 2508 (2012).

[18] C. Klingner, C. Krellner, M. Brando, C. Geibel, and F. Steglich, Magnetic behaviour of the intermetallic compound $YbCo_2Si_2$, New J. Phys. **13**, 083024 (2011).

[19] See Supplemental Material at http://link.aps.org/supplemental/10.1103/PhysRevB.109.L241118 for the theory of RPED and additional information, which includes Ref. [36].

[20] H. Ogasawara and A. Kotani, Calculation of rare-earth $4d$ giant-absorption spectra with multiplet effects and decay processes, J. Synchrotron Radiat. **8**, 220 (2001).

[21] D. Y. Usachov, D. Glazkova, A. V. Tarasov, S. Schulz, G. Poelchen, K. A. Bokai, O. Y. Vilkov, P. Dudin, K. Kummer, K. Kliemt, C. Krellner, and D. V. Vyalikh, Estimating the orientation of $4f$ magnetic moments by classical photoemission, J. Phys. Chem. Lett. **13**, 7861 (2022).

[22] V. F. Bratzev, G. B. Deyneka, and I. I. Tupitsyn, Application of the Hartree-Fock method to calculation of relativistic atomic wave functions, Bull. Acad. Sci. USSR. Phys. Ser. **41**, 173 (1977).

[23] F. J. García de Abajo, M. A. Van Hove, and C. S. Fadley, Multiple scattering of electrons in solids and molecules: A cluster-model approach, Phys. Rev. B **63**, 075404 (2001).

[24] S. Danzenbächer, D. V. Vyalikh, K. Kummer, C. Krellner, M. Holder, M. Höppner, Y. Kucherenko, C. Geibel, M. Shi, L. Patthey, S. L. Molodtsov, and C. Laubschat, Insight into the f-derived Fermi surface of the heavy-fermion compound YbRh$_2$Si$_2$, Phys. Rev. Lett. **107**, 267601 (2011).

[25] D. V. Vyalikh, S. Danzenbächer, Y. Kucherenko, K. Kummer, C. Krellner, C. Geibel, M. G. Holder, T. K. Kim, C. Laubschat, M. Shi, L. Patthey, R. Follath, and S. L. Molodtsov, k dependence of the crystal-field splittings of $4f$ states in rare-earth systems, Phys. Rev. Lett. **105**, 237601 (2010).

[26] S. Danzenbächer, Y. Kucherenko, D. V. Vyalikh, M. Holder, C. Laubschat, A. N. Yaresko, C. Krellner, Z. Hossain, C. Geibel, X. J. Zhou, W. L. Yang, N. Mannella, Z. Hussain, Z.-X. Shen, M. Shi, L. Patthey, and S. L. Molodtsov, Momentum dependence of $4f$ hybridization in heavy-fermion compounds: Angle-resolved photoemission study of YbIr$_2$Si$_2$ and YbRh$_2$Si$_2$, Phys. Rev. B **75**, 045109 (2007).

[27] K. Kummer, Y. Kucherenko, S. Danzenbächer, C. Krellner, C. Geibel, M. G. Holder, L. V. Bekenov, T. Muro, Y. Kato, T. Kinoshita, S. Huotari, L. Simonelli, S. L. Molodtsov, C. Laubschat, and D. V. Vyalikh, Intermediate valence in Yb compounds probed by $4f$ photoemission and resonant inelastic x-ray scattering, Phys. Rev. B **84**, 245114 (2011).

[28] A. S. Kutuzov and A. M. Skvortsova, Crystal electric field parameters for Yb^{3+} ion in YbRh$_2$Si$_2$, J. Phys.: Conf. Ser. **324**, 012039 (2011).

[29] A. Leushin and V. Ivanshin, Crystalline electric fields and the ground state of YbRh$_2$Si$_2$ and YbIr$_2$Si$_2$, Phys. B: Condens. Matter **403**, 1265 (2008).

[30] A. V. Tarasov, D. Glazkova, S. Schulz, G. Poelchen, K. Kliemt, A. Kraiker, M. Muntwiler, C. Laubschat, A. Generalov, C. Polley, C. Krellner, D. V. Vyalikh, and D. Y. Usachov, Crystal electric field and properties of $4f$ magnetic moments at the surface of the rare-earth compound TbRh$_2$Si$_2$, Phys. Rev. B **106**, 155136 (2022).

[31] D. Y. Usachov, A. V. Tarasov, D. Glazkova, M. Mende, S. Schulz, G. Poelchen, A. V. Fedorov, O. Y. Vilkov, K. A. Bokai, V. S. Stolyarov, K. Kliemt, C. Krellner, and D. V. Vyalikh, Insight into the temperature-dependent canting of $4f$ magnetic moments from $4f$ photoemission, J. Phys. Chem. Lett. **14**, 5557 (2023).

[32] D. Y. Usachov, A. V. Tarasov, K. A. Bokai, V. O. Shevelev, O. Y. Vilkov, A. E. Petukhov, A. G. Rybkin, I. I. Ogorodnikov, M. V. Kuznetsov, M. Muntwiler, F. Matsui, L. V. Yashina, C. Laubschat, and D. V. Vyalikh, Site- and spin-dependent coupling at the highly ordered h-BN/Co(0001) interface, Phys. Rev. B **98**, 195438 (2018).

[33] E. A. Goremychkin and R. Osborn, Crystal field excitations in YbT$_2$Si$_2$ (T = Fe, Co, Ni), J. Appl. Phys. **87**, 6818 (2000).

[34] T. Gruner, J. Sichelschmidt, C. Klingner, C. Krellner, C. Geibel, and F. Steglich, Electron spin resonance of the Yb $4f$ moment in Yb(Rh$_{1-x}$Co$_x$)$_2$Si$_2$, Phys. Rev. B **85**, 035119 (2012).

[35] G. van der Laan, E. Arenholz, Z. Hu, A. Bauer, E. Weschke, C. Schüssler-Langeheine, E. Navas, A. Mühlig, G. Kaindl, J. B. Goedkoop, and N. B. Brookes, Magnetic circular dichroism in Tb $3d \rightarrow 4f$ resonant photoemission, Phys. Rev. B **59**, 8835 (1999).

[36] M. P. Seah and W. A. Dench, Quantitative electron spectroscopy of surfaces: A standard data base for electron inelastic mean free paths in solids, Surf. Interf. Anal. **1**, 2 (1979).